crystals

MDPI

Article

Selection Criterion of Stable Dendritic Growth for a Ternary (Multicomponent) Melt with a Forced Convective Flow

Dmitri V. Alexandrov [1], Sergei I. Osipov [2], Peter K. Galenko [3] and Liubov V. Toropova [3,4,*]

[1] Laboratory of Multi-Scale Mathematical Modeling, Department of Theoretical and Mathematical Physics, Ural Federal University, Lenin Ave., 51, 620000 Ekaterinburg, Russia
[2] Institute of Natural Sciences and Mathematics, Ural Federal University, Lenin Ave., 51, 620000 Ekaterinburg, Russia
[3] Otto-Schott-Institut für Materialforschung, Friedrich-Schiller-Universität-Jena, 07743 Jena, Germany
[4] Laboratory of Mathematical Modeling of Physical and Chemical Processes in Multiphase Media, Department of Theoretical and Mathematical Physics, Ural Federal University, 620000 Ekaterinburg, Russia
* Correspondence: l.v.toropova@urfu.ru

Abstract: A stable growth mode of a single dendritic crystal solidifying in an undercooled ternary (multicomponent) melt is studied with allowance for a forced convective flow. The steady-state temperature, solute concentrations and fluid velocity components are found for two- and three-dimensional problems. The stability criterion and the total undercooling balance are derived accounting for surface tension anisotropy at the solid-melt interface. The theory under consideration is compared with experimental data and phase-field modeling for $Ni_{98}Zr_1Al_1$ alloy.

Keywords: dendrites; stable growth; selection criterion; solvability theory; morphological stability; forced convective flow; undercooling balance; multicomponent melt

Citation: Alexandrov, D.V.; Osipov, S.I.; Galenko, P.K.; Toropova, L.V. Selection Criterion of Stable Dendritic Growth for a Ternary (Multicomponent) Melt with a Forced Convective Flow. *Crystals* **2022**, *12*, 1288. https://doi.org/10.3390/cryst12091288

Academic Editor: Cyril Cayron

Received: 22 August 2022
Accepted: 8 September 2022
Published: 12 September 2022

1. Introduction

Solidification phenomena have a very important role in metallurgy and in some cases fully determine the physical and mechanical features of a solidified substance. Mathematical models of such phenomena stem from the classical Stefan model that describes crystallization with a flat boundary [1–3]. However, such a crystallization scenario is rarely realized in practical conditions. Usually, a flat boundary is destroyed due to the thermal or concentration undercooling [4–8]. Concentration undercooling, which appears at the crystallization interface (when the concentration gradient exceeds the temperature gradient), leads to favorable conditions for the growth of individual solid phase ridges, which create an extended area for dendritic growth ahead of the solid-liquid phase boundary known as a mushy layer [9–12]. In this layer, the evolution of dendrite-like structures, nucleation and growth of crystals are possible to observe [13–17].

The problem for the selection of a stable dendrite growth regime in the melt has arisen from the analysis of Ivantsov solutions [18–20] and experiments for a parabolic needle-shaped crystal [21–27]. These comparisons and tests have led to the conclusion that the continuous family of isotropic Ivantsov thermal and solute concentration distributions is unstable: the needle crystal loses its initial parabolic shape in the steady-state growth regime (see, among others, [28]). Therefore the Ivantsov solution is used as the main approximation for the analysis of stable growth, where the role of a small parameter is played by the surface tension anisotropy or the growth kinetics anisotropy [29,30]. After establishing the criterion for steady growth of a dendrite vertex in a single-component medium [28,29], the problem has been extended to the case of convective motion of the medium [31], to the case of dendrite growth in a binary system without convection [32] and to the case of dendrite growth in a binary system with convection [33]. Then, this theory was developed for rapid dendritic growth phenomena [34,35]. In many circumstances, however,

a comparative analysis of dendrite growth should be carried out taking into account the multi-component nature of the system [36,37]. In the present paper, which continues and develops the aforementioned studies, the effect of three-component (multicomponent) melt when considering the the stable mode of dendritic growth with a forced flow is investigated.

2. The Model of Dendritic Growth

The growth of dendritic tip moving deep into the undercooled ternary melt is characterized by a nonlinear moving-boundary problem with a curvilinear solid/liquid interface (a sketch of the process is demonstrated in Figure 1). As this takes place, the interfacial temperature θ_{int} for a one-component melt is defined by the interface local curvature $\mathcal{K}$, the phase transition temperature of planar boundary θ_*, the adiabatic temperature $\theta_Q = Q/\kappa_p$ and the capillary length d

$$\theta_{\text{int}} = \theta_* - \theta_Q d\mathcal{K}, \tag{1}$$

where Q represents the latent heat of solidification, κ_p is the specific heat, and d is a function of polar angle θ shown (Figure 1) defined as [20,29]

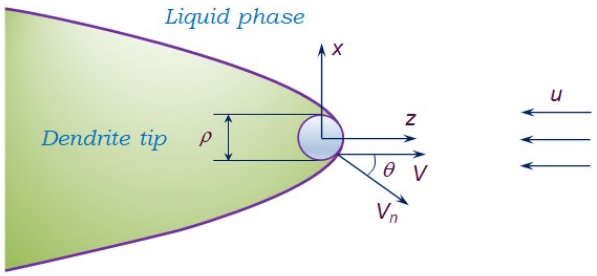

Figure 1. A sketch of dendritic tip with incoming melt flow.

$$d(\theta) = d_0\{1 - \chi_d \cos[n(\theta - \theta_d)]\}, \tag{2}$$

where d_0 is the capillary constant. It should be especially emphasized that Equation (2) takes place for n-fold crystal symmetry. The constant parameter χ_d is estimated to be significantly less than one. In addition, it should be mentioned that the solid/liquid interface curvature $\mathcal{K}$ is $2/\rho$ and $4/\rho$ in the two- and three-dimensional dendrite growth geometries, respectively [38] (ρ represents the crystal tip diameter). An important point is that the misalignment angle θ_d is negligibly small [20,29].

The temperature field in the solid (θ_s) and liquid (θ_l) phases with allowance for melt convection is described by equations

$$\frac{\partial \theta_s}{\partial \tau} = D_\theta \nabla^2 \theta_s \ \ (\text{solid phase}), \tag{3}$$

$$\frac{\partial \theta_l}{\partial \tau} + (\mathbf{v} \cdot \nabla)\theta_l = D_\theta \nabla^2 \theta_l, \ \ (\text{liquid phase}). \tag{4}$$

Here, τ is the process time, D_θ is the temperature diffusivity, and $\mathbf{v}$ is the melt velocity. Let us especially underline that the temperature diffusivities in expressions (3) and (4) are chosen to be equal. This is traditionally used in the selection theory of a stable mode of dendritic growth [20,28–33]. If we would choose different temperature diffusivities in Equations (3) and (4), this would greatly complicate the mathematical transformation, but would not change the final selection criterion, because only the constant σ_{0n} in expression (26) would change.

The solute concentrations σ_1 and σ_2 of dissolved impurities in a ternary melt satisfy the diffusion equations [39–43]

$$\frac{\partial \sigma_1}{\partial \tau} + (\mathbf{v} \cdot \nabla)\sigma_1 = D_1 \nabla^2 \sigma_1, \quad \frac{\partial \sigma_2}{\partial \tau} + (\mathbf{v} \cdot \nabla)\sigma_2 = D_2 \nabla^2 \sigma_2 \quad \text{(liquid phase)}, \tag{5}$$

where D_1 and D_2 are the diffusion coefficients of corresponding dissolved impurities.Let us especially highlight that the diffusion coefficients in Equation (5) should be different because both dissolved impurities in the melt diffuse at different rates.

At the moving dendrite interface with a constant velocity v, we have the equality of temperatures in solid and liquid phases to the phase transition temperature dependent of solute concentrations as well as the heat and mass balances [40–43], i.e.,

$$\theta_s = \theta_l = \theta_{\text{int}} - m_1 \sigma_1 - m_2 \sigma_2, \quad \text{(at the interface)}, \tag{6}$$

$$\frac{Q}{D_\theta \kappa_p} \mathbf{V} \cdot \mathbf{n} = (\nabla \theta_s - \nabla \theta_l) \cdot \mathbf{n}, \quad \text{(at the interface)}, \tag{7}$$

$$(1 - k_{1,2})\sigma_{1,2} \mathbf{V} \cdot \mathbf{n} + D_{1,2} \nabla \sigma_{1,2} \cdot \mathbf{n} = 0, \quad \text{(at the interface)}, \tag{8}$$

where m_1 and m_2 represent the liquidus slopes determined from the phase diagram, $\mathbf{V} \cdot \mathbf{n}$ is the normal growth velocity, k_1 and k_2 are the partition coefficients corresponding to the solute concentrations σ_1 and σ_2.

In addition, we assume that the temperature and solute concentrations at infinity are known, i.e.,

$$\theta_l \to \theta_\infty, \quad \sigma_1 \to \sigma_{1\infty}, \quad \sigma_2 \to \sigma_{2\infty} \quad \text{(far from the crystal)}. \tag{9}$$

Accounting for the melt viscosity and simplifying the matter, we use the Oseen hydrodynamic model as follows [44–46]

$$u \frac{\partial \mathbf{v}}{\partial z} = -\frac{1}{\rho_m} \nabla p + \mu \Delta \mathbf{v}, \quad \nabla \cdot \mathbf{v} = 0, \quad \text{(liquid phase)}, \tag{10}$$

where u is the velocity of undercooled melt far from the dendrite at $z \to \infty$ (Figure 1), ρ_m is the density of undercooled ternary melt, p is the liquid-phase pressure, and μ is the melt viscosity.

Equations (10) should be supplemented with the adhesion condition of liquid particles to the dendrite surface. Note that the hydrodynamic problem based on Equation (10) has been previously solved in Refs. [47,48]. Below, we use this solution, referring the interested reader to the original solution developed in Refs. [47,48].

3. Analytical Solutions for Steady-State Dendritic Growth

The aforementioned governing equations and boundary conditions can be solved in parabolic (paraboloidal) coordinates, which follow isothermal (isoconcentration) surfaces $\zeta = \text{const.}$ around the dendritic vertex (Figure 2).

Thus, instead of Cartesian coordinates x, y and z, we use the curvilinear coordinates ζ, ξ (and ϕ in 3D).

$$\begin{gathered} z = \frac{\rho(\zeta - \xi)}{2}, \quad x = \rho(\xi\zeta)^{1/2} \ \text{in 2D}, \\ z = \frac{\rho(\zeta - \xi)}{2}, \quad x = \rho(\xi\zeta)^{1/2} \cos\phi, \quad y = \rho(\xi\zeta)^{1/2} \sin\phi \ \text{in 3D}. \end{gathered} \tag{11}$$

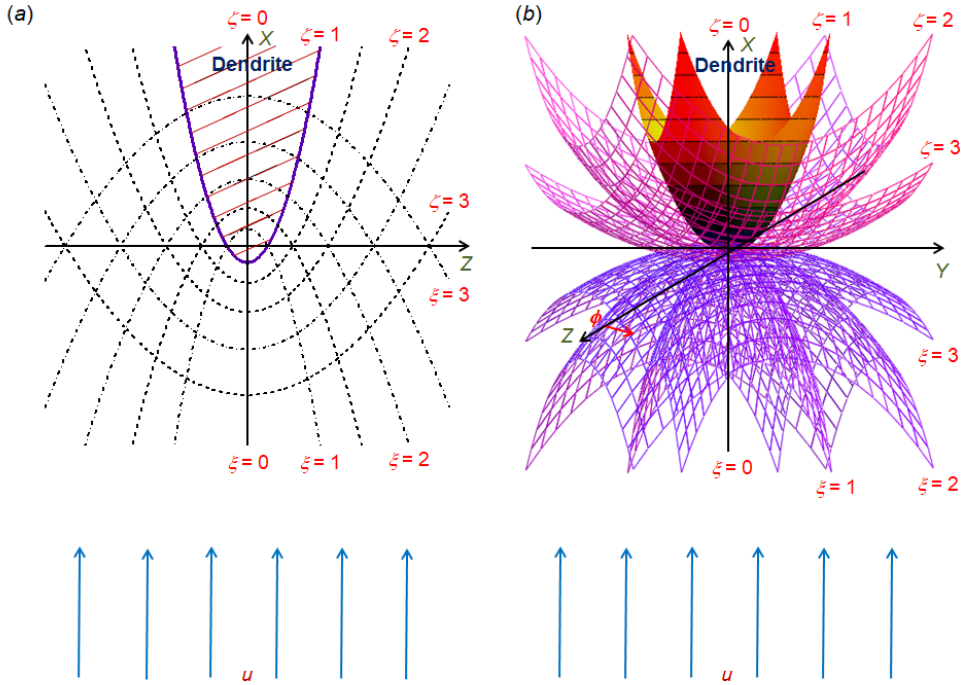

Figure 2. A scheme of a dendritic vertex swept by an undercooled melt (2D in (**a**) and 3D in (**b**)). The figure shows the dendrite vertex and the isothermal (isoconcentration) surfaces $\zeta = \text{const.}$ around it.

We seek for a steady-state solution for the dendrite tip moving with a constant velocity v upstream of the melt flow (Figure 1). The process is established and temperature and solute concentrations are dependent only on ζ, i.e., $\theta_l = \theta_l(\zeta)$, and $\sigma_{1,2} = \sigma_{1,2}(\zeta)$. Assuming that the temperature in solid does not change, we arrive at the steady-state temperature and solute concentration profiles in the melt phase

$$\theta_l(\zeta) = \theta_i + \frac{(\theta_\infty - \theta_i) I_\theta(\zeta)}{I_\theta(\infty)},$$
$$\sigma_1(\zeta) = \sigma_{1i} + \frac{(\sigma_{1\infty} - \sigma_{1i}) I_{1\sigma}(\zeta)}{I_{1\sigma}(\infty)}, \quad \sigma_2(\zeta) = \sigma_{2i} + \frac{(\sigma_{2\infty} - \sigma_{2i}) I_{2\sigma}(\zeta)}{I_{2\sigma}(\infty)}, \tag{12}$$

where θ_i, σ_{1i} and σ_{2i} represent the interfacial temperature and solute concentrations (at $\zeta = 1$) and have the form

$$\theta_i = \theta_\infty + \theta_Q P_\theta \exp(P_0) I_\theta(\infty),$$
$$\sigma_{1i} = \frac{\sigma_{1\infty}}{1 - (1 - k_1)\exp(P_0 D_\theta / D_1) P_\theta I_{1\sigma}(\infty) D_\theta / D_1},$$
$$\sigma_{2i} = \frac{\sigma_{2\infty}}{1 - (1 - k_2)\exp(P_0 D_\theta / D_2) P_\theta I_{2\sigma}(\infty) D_\theta / D_2},$$
$$I_\theta(\zeta) = \int_1^\zeta \exp\left[(k-1)P_u \int_1^{\zeta_1} \frac{G(\zeta_2) d\zeta_2}{\sqrt{\zeta_2}} - P_0 \zeta_1\right] \frac{d\zeta_1}{\zeta_1^{(k-1)/2}},$$
$$I_{1\sigma}(\zeta) = \int_1^\zeta \exp\left[(k-1)P_u \frac{D_\theta}{D_1} \int_1^{\zeta_1} \frac{G(\zeta_2) d\zeta_2}{\sqrt{\zeta_2}} - P_0 \frac{D_\theta}{D_1} \zeta_1\right] \frac{d\zeta_1}{\zeta_1^{(k-1)/2}},$$
$$I_{2\sigma}(\zeta) = \int_1^\zeta \exp\left[(k-1)P_u \frac{D_\theta}{D_2} \int_1^{\zeta_1} \frac{G(\zeta_2) d\zeta_2}{\sqrt{\zeta_2}} - P_0 \frac{D_\theta}{D_2} \zeta_1\right] \frac{d\zeta_1}{\zeta_1^{(k-1)/2}},$$

where $k = 2$ in the case of two-dimensional growth and $k = 3$ in three dimensional space. Here, $G(\zeta)$ follows from the Oseen hydrodynamic equations and has the form [47,48]

$$G(\zeta) = \frac{\operatorname{erfc}\sqrt{\zeta\Re/2}}{\operatorname{erfc}\sqrt{\Re/2}}\sqrt{\zeta} + \frac{\sqrt{2}}{\sqrt{\pi\Re}\operatorname{erfc}\sqrt{\Re/2}}\left[\exp\left(-\frac{\Re}{2}\right) - \exp\left(-\frac{\zeta\Re}{2}\right)\right] \text{ in 2D,}$$

$$G(\zeta) = \frac{\sqrt{\zeta}E_1(\zeta\Re/2)}{2E_1(\Re/2)} + \frac{\exp(-\Re/2) - \exp(-\zeta\Re/2)}{\sqrt{\zeta}\Re E_1(\Re/2)} \text{ in 3D,}$$

where $\Re = \rho u/\mu$ represents the Reynolds number, and $E_1(b) = \int_b^\infty \gamma^{-1}\exp(-\gamma)d\gamma$. In addition, P_θ and P_u represent the thermal and flow Péclet numbers

$$P_\theta = \frac{\rho V}{2D_\theta}, \; P_u = \frac{\rho u}{2D_\theta} \text{ and } P_0 = P_\theta + P_u.$$

4. The Total Melt Undercooling

The total melt undercooling $\Delta\theta = \theta_* - \theta_\infty - m_1\sigma_{1\infty} - m_2\sigma_{2\infty}$ is the reason of dendritic growth and solidification phenomenon. This undercooling contains several contributions stemming from the temperature difference ($\Delta\theta_\theta$—thermal undercooling), displacement of imputiries ($\Delta\theta_\sigma$—concentration undercooling) and curvilinear crystal shape ($\Delta\theta_\rho$ shape undercooling)

$$\Delta\theta = \Delta\theta_\theta + \Delta\theta_\sigma + \Delta\theta_\rho. \tag{13}$$

These undercooling contributions are dependent on crystal tip diameter ρ and its velocity V.

So, the first of them is given by

$$\Delta\theta_\theta(\rho, V) = \theta_i - \theta_\infty = \theta_Q \mathrm{Iv}^*_\theta(\rho, V). \tag{14}$$

The second one reads as

$$\begin{aligned}\Delta\theta_\sigma(\rho, V) &= m_1(\sigma_{1i} - \sigma_{1\infty}) + m_2(\sigma_{2i} - \sigma_{2\infty}) \\ &= \frac{m_1\sigma_{1\infty}(1-k_1)\mathrm{Iv}^*_{\sigma 1}(\rho, V)}{1-(1-k_1)\mathrm{Iv}^*_{\sigma 1}(\rho, V)} + \frac{m_2\sigma_{2\infty}(1-k_2)\mathrm{Iv}^*_{\sigma 2}(\rho, V)}{1-(1-k_2)\mathrm{Iv}^*_{\sigma 2}(\rho, V)}.\end{aligned} \tag{15}$$

Here, the thermal and concentration Ivantsov integrals are

$$\mathrm{Iv}^*_\theta(\rho, V) = P_\theta(\rho, V)\exp[P_0(\rho, V)]I_\theta(\infty),$$

$$\mathrm{Iv}^*_{\sigma 1}(\rho, V) = P_\theta(\rho, V)\frac{D_\theta}{D_1}\exp\left[\frac{P_0(\rho, V)D_\theta}{D_1}\right]I_{1\sigma}(\infty),$$

$$\mathrm{Iv}^*_{\sigma 2}(\rho, V) = P_\theta(\rho, V)\frac{D_\theta}{D_2}\exp\left[\frac{P_0(\rho, V)D_\theta}{D_2}\right]I_{2\sigma}(\infty).$$

The third contribution has the form

$$\Delta\theta_\rho(\rho) = \frac{2d_0\theta_Q}{\rho} \text{ (2D) and } \Delta\theta_\rho(\rho) = \frac{4d_0\theta_Q}{\rho} \text{ (3D).} \tag{16}$$

The total undercooling (13) is a function of ρ and V. To obtain $\rho(\Delta\theta)$ and $V(\Delta\theta)$, we need one more condition that connects these the variables. Such a condition (selection criterion) follows from the solvability theory and morphological stability analysis developed below.

5. Selection Criterion for Stable Dendritic Growth

To derive the selection criterion we shall use the microscopic solvability condition. By substituting the marginal mode of the wavenumber κ_m into this condition, we obtain a

criterion for the selection of a stable growth mode of dendrite vertex. Let us write down this condition as [2,49]

$$\int_{-\infty}^{\infty} A[\Xi_0(\ell)]\wp_m(\ell)d\ell = 0, \;\; \wp_m(\ell) = \exp\left[i\int_0^{\ell}\kappa_m(\ell_1)d\ell_1\right], \tag{17}$$

where A stands for the curvature operator, $\Xi_0(\ell)$ represents the solution of moving-boundary problem, and i is the imaginary unit. It is significant to note that expression (17) represents an additional condition connecting three main growth parameters: dendrite tip diameter ρ, dendrite tip velocity V and melt undercooling $\Delta\theta$.

Our subsequent analysis builds on the theory developed by Bouissou and Pelcé [31]. According to this theory, we expand in Taylor series the components of fluid velocity in the neighbourhood of the dendrite surface $\zeta = 1$

$$u_\zeta = -V(\xi+1)^{-1/2}, \;\; u_\xi = \left(\frac{\xi}{\xi+1}\right)^{1/2}(V + b(\Re)u(\zeta-1)), \tag{18}$$

where

$$b(\Re) = \left(\frac{\Re}{2\pi}\right)^{1/2}\frac{\exp(-\Re/2)}{\mathrm{erfc}\,(\sqrt{\Re/2})} \;\text{ in 2D and }\; b(\Re) = \frac{\exp(-\Re/2)}{E_1(\Re/2)} \;\text{ in 3D.}$$

in addition, we introduce the orthogonal coordinate system (x_l, y_l) linked to the moving dendrite surface [31] (x_l and y_l are the tangent and normal axes, respectively). Taking this into account we represent expressions (18) in the form of

$$\tilde{v} = -V\cos\theta, \;\; \tilde{u} = -V\sin\theta - \frac{b(\Re)u\sin(2\theta)}{2\rho}y_l, \tag{19}$$

where $\tilde{u}$ and $\tilde{v}$ stand for the tangent and normal velocities in the vicinity of growing crystal.

Expressions (7) and (8) lead to the temperature and solute concentrations derivatives at the crystal boundary $y_l = 0$

$$\frac{d\tilde{\theta}_l}{dy_l} = -\frac{\theta_Q V\cos\theta}{D_\theta}, \;\; \frac{d\tilde{\sigma}_1}{dy_l} = \frac{(k_1-1)V\sigma_{1i}\cos\theta}{D_1}, \;\; \frac{d\tilde{\sigma}_2}{dy_l} = \frac{(k_2-1)V\sigma_{2i}\cos\theta}{D_2}, \;\; y_l = 0. \tag{20}$$

Here, the symbol "tilde" designates the stationary solutions. Bearing this in mind we obtain the temperature and solute concentrations in the vicinity of dendritic boundary

$$\tilde{\theta}_l = \theta_i - \frac{\theta_Q V\cos\theta}{D_\theta}y_l, \;\; \tilde{\sigma}_1 = \sigma_{1i} + \frac{(k_1-1)V\sigma_{1i}\cos\theta}{D_1}y_l, \;\; \tilde{\sigma}_2 = \sigma_{2i} + \frac{(k_2-1)V\sigma_{2i}\cos\theta}{D_2}y_l. \tag{21}$$

Let the solid/liquid interface undergoes morphological perturbations Σ'. By this is meant that the temperature and concentration fields also undergo perturbations θ_s', θ_l', σ_1' and σ_2'. Perturbations also take place in the fluid velocity components u' and v' and pressure p'. All of these perturbations are considered to be sufficiently small as compared to the stationary solutions.

The heat and mass transfer Equations (3)–(5) lead us to the equations for perturbations, which read as

$$\begin{gathered}\frac{\partial\theta_s'}{\partial\tau} + \tilde{u}\frac{\partial\theta_s'}{\partial x_l} + \tilde{v}\frac{\partial\theta_s'}{\partial y_l} + v'\frac{d\tilde{\theta}_s}{dy_l} = D_\theta\nabla^2\theta_s', \;\; \frac{\partial\theta_l'}{\partial\tau} + \tilde{u}\frac{\partial\theta_l'}{\partial x_l} + \tilde{v}\frac{\partial\theta_l'}{\partial y_l} + v'\frac{d\tilde{\theta}_l}{dy_l} = D_\theta\nabla^2\theta_l', \\ \frac{\partial\sigma_1'}{\partial\tau} + \tilde{u}\frac{\partial\sigma_1'}{\partial x_l} + \tilde{v}\frac{\partial\sigma_1'}{\partial y_l} + v'\frac{d\tilde{\sigma}_1}{dy_l} = D_1\nabla^2\sigma_1', \;\; \frac{\partial\sigma_2'}{\partial\tau} + \tilde{u}\frac{\partial\sigma_2'}{\partial x_l} + \tilde{v}\frac{\partial\sigma_2'}{\partial y_l} + v'\frac{d\tilde{\sigma}_2}{dy_l} = D_2\nabla^2\sigma_2', \\ \nabla p' - \mu\rho_m\Delta\mathbf{v}' = 0, \;\; \nabla\cdot\mathbf{v}' = 0.\end{gathered} \tag{22}$$

Here, the symbol $'$ designates the perturbations.

Expanding the boundary conditions (6)–(8) in series in the vicinity of crystal boundary $y_l = 0$, we come to

$$\begin{gathered}\theta_s' = \frac{\theta_Q V\cos\theta}{D_\theta}\Sigma' - \theta_l',\\ \theta_s' + \frac{m_1\sigma_{1i}(1-k_1)V\cos\theta}{D_1}\Sigma' + \frac{m_2\sigma_{2i}(1-k_2)V\cos\theta}{D_2}\Sigma' = \theta_Q d(\theta)\frac{\partial^2\Sigma'}{\partial y_l^2} + m_1\sigma_1' + m_2\sigma_2',\\ v' = -\frac{\partial\Sigma'}{\partial\tau},\ \ u' = 0,\ \ \frac{\theta_Q}{D_\theta}\frac{\partial\Sigma'}{\partial\tau} + \frac{\partial\theta_l'}{\partial y_l} + \frac{\theta_Q V^2\cos^2\theta}{D_\theta^2}\Sigma' = \frac{\partial\theta_s'}{\partial y_l}.\end{gathered} \tag{23}$$

An important point is that the morphological perturbations represent an exponential function of the form

$$\exp(\varpi\tau + i\kappa x_l - \varepsilon\kappa y_l) \tag{24}$$

when dealing with the linear stability analysis. Note that ϖ and κ represent the frequency and wavenumber, whereas $|\varepsilon| = 1$ describes the decay of perturbations at infinity, i.e., at $y_l \to \infty$.

Below, we assume that the morphological perturbations have the exponential form (24). Substituting them into conditions (23) we arrive at equations for their amplitudes. By equating the determinant of the system of equations for the perturbation amplitudes to zero, we construct a non-trivial solution. This leads us to the equation for the marginal wavenumber $\kappa = \kappa_m$

$$\begin{gathered}\kappa_m^3 - \left(\frac{V}{2D_\theta d(\theta)} + \frac{m_1(1-k_1)\sigma_{1i}V}{\theta_Q D_1 d(\theta)} + \frac{m_2(1-k_2)\sigma_{2i}V}{\theta_Q D_2 d(\theta)}\right)\exp(i\theta)\kappa_m - \frac{ib(\Re)u\sin(2\theta)}{16\rho D_\theta}\kappa_m\\ -\frac{ib(\Re)u\sin(2\theta)}{8\rho D_1}\kappa_m - \frac{ib(\Re)u\sin(2\theta)}{8\rho D_2}\kappa_m + \frac{iV\sin\theta}{2D_\theta}\kappa_m^2 - \frac{V^2\cos\theta\exp(i\theta)}{4D_\theta^2 d(\theta)} = 0.\end{gathered} \tag{25}$$

Here, we assume that the stationary dendrite evolves with the rate $-i\kappa V\sin\theta$. By this is meant that the perturbation grows with the rate $\varpi(\kappa)$. Thus, the rate of morphological perturbation behaves as a sum of these functions, i.e., $\varpi(\kappa) - iV\kappa\sin\theta$. It is significant that we assume here the constant dendritic rate V. This rate can be attained quickly enough in real growth processes [50]. In addition, expression (25) has been derived for the neutral stability curve $\varpi = 0$ with allowance for $\varepsilon = -1$ (also, i was replaced by $-i$, [31]). The marginal mode of the wavenumber (25) contains all limiting transitions to previous studies [2,31–33,49,51–56] devoted to simpler cases of dendritic growth.

Now, substituting the wavenumber from expression (25) into the solvability condition (17), we obtain

$$\begin{gathered}\sigma^* \equiv \frac{2d_0D_\theta}{\rho^2V} = \frac{\sigma_{0n}\chi_d^{7/n}B_n^{7/n}}{1+\beta\bar{v}_n^{s_n}}\left\{\frac{1}{\left[1+b_{1n}\chi_d^{2/n}B_n^{2/n}P_\theta\right]^2}\right.\\ \left.+\frac{2(1-k_1)m_1\sigma_{1i}D_\theta}{\left[1+b_{2n}\chi_d^{2/n}B_n^{2/n}P_{1\sigma}\right]^2D_1\theta_Q} + \frac{2(1-k_2)m_2\sigma_{2i}D_\theta}{\left[1+b_{2n}\chi_d^{2/n}B_n^{2/n}P_{2\sigma}\right]^2D_2\theta_Q}\right\},\end{gathered} \tag{26}$$

where

$$\bar{v}_n = \left(\frac{b(\Re)ud_0}{4V\rho R} + \frac{b(\Re)ud_0D_\theta}{2V\rho RD_1} + \frac{b(\Re)ud_0D_\theta}{2V\rho RD_2}\right)\chi_d^{-3/n}B_n^{-3/n},\ \ s_n = \frac{n+7}{2(n+3)},$$

$$R = 1 + \frac{2(1-k_1)m_1\sigma_{1i}D_\theta}{D_1\theta_Q} + \frac{2(1-k_2)m_2\sigma_{2i}D_\theta}{D_2\theta_Q}, \quad b_{2n} = b_{1n}\sqrt{2},$$

$$b_{1n} = B_n^{3/2n}\chi_d^{3/2n-3/8}\left(\frac{8\sigma_{0n}}{7}\right)^{1/2}\left(\frac{3}{56}\right)^{3/8}, \quad B_n = 2^{-3n/4}\sum_{j=0}^{n}\binom{n}{j}i^{n-j}\cos\frac{\pi(n-j)}{2},$$

where σ_{0n} is the selection constant characterizing the stable evolution of dendrites without forced convection, β is the selection constant if considering convection in a pure system, $P_\theta = \rho V/(2D_\theta)$ is the thermal Péclet number, $P_{1\sigma} = \rho V/(2D_1)$ and $P_{2\sigma} = \rho V/(2D_2)$ are the concentration Péclet numbers.

Expression (26) represents the selection criterion in the case of ternary melt with convection. It defines an additional relation between ρ, V and $\Delta\theta$ so that the undercooling balance (14) and selection criterion (26) represent two nonlinear equations leading to $\rho(\Delta\theta)$ and $V(\Delta\theta)$. It is significant that criterion (26) has limiting transitions to previous theories [2,31–33,49,51–56] devoted to simpler cases. As a special note, we note that the selection criterion (26) coincides with the previously developed criterion for a ternary system with four-fold crystalline symmetry without convection [57]. Moreover, a generalized selection criterion (26) for the N-component dilute melt is presented in Appendix A.

6. A Test of Theory against Experimental Data and Phase-Field Modeling for $Ni_{98}Zr_1Al_1$ Alloy

The experiments for detecting dendritic growth velocities of $Ni_{98}Zr_1Al_1$ alloy [58] were carried out using an electromagnetic levitation facility [56]. The sample temperature during solidification was measured with a two-color pyrometer, recorded using a transient recorder, and, in addition, the solidification process was observed by a high-speed camera. Further, growth velocity measurments were evaluated in solidified samples described by steady-state dendritic growth where the growth front is depicted by the intersection of the envelope of all dendrites with the sample surface. Figure 3 represents a good match of calculated theoretical results together with the obtained experimental data [58] of dendritic growth velocity as a function of melt undercooling (material and calculation parameters for the alloy $Ni_{98}Zr_1Al_1$ are given in Table 1). Even though the dendritic growth velocity is predicted for the whole range of undercoolings (see Figure 3), the theoretical curve overestimates the experimental data within the experimental margin of error in the region of diffusion-limited growth with $\Delta\theta \approx 70$ K. One reason for such a disagreement could be the dependency of the solute partitioning and the liquidus slope on the temperature and composition in the multicomponent alloy system.

Table 1. Material and calculation parameters for the alloy $Ni_{98}Zr_1Al_1$. Subscripts *Zr* and *Al* correspond to subscripts 1 and 2 in formulas (lines marked by *).

Parameter	Symbol	Value	Units
Solute partition coefficient *	k_{Zr}/k_{Al}	0.013/1.133	-
Liquidus slope *	m_{Zr}/m_{Al}	−18.58/0.18	K/at.%
Solute diffusion coefficient *	D_{CZr}/D_{CAl}	$2.1\times10^{-9}/2.1\times10^{-9}$	$m^2\ s^{-1}$
Initial composition *	σ_{Zr}/σ_{Al}	1/1	at.%
Thermal diffusivity	D_θ	1.2×10^{-5}	$m^2\ s^{-1}$
Hypercooling	θ_Q	656	K
Liquidus temperature	θ_*	1728	K
Capillary constant	d_0	3.28×10^{-10}	m
Specific heat	κ_p	41	$J\ mol^{-1}\ K^{-1}$
Surface energy stiffness	χ_d	0.021	-
Solvability constant	σ_{0n}	0.3	-
Order of crystalline symmetry	n	4	-

In addition to the experimental data, phase-field is often used to test the accuracy of theoretical models. Nowadays, the application of the phase-field method to predict the formation and evolution of microstructures is undergoing a remarkable development. For instance, the phase-field modeling (PFM) can be used to study the multi-controlling factors of dendrite growth in directional solidification [59] and for describing the evolution of complex typical and atypical types of dendrite morphology observed during solidification of Al-Zn alloys [60]. Here, a general multicomponent multiphase field model was applied for the direct simulation of dendritic growth structures. This model and its implementation allow online coupling to thermodynamic databases and, consequently, make it possible to take into account the temperature and compositional dependence of the solute distribution at the interface (see for details [61]). Figure 3 compares the model predictions of thedendritic tip velocity and dendritic diameter as a function of undercooling and the star indicates the result of three-dimensional phase-field modeling [58]. As it can be easily seen a good agreement between our calculated results and PFM modeling was achieved for $Ni_{98}Zr_1Al_1$ alloy.

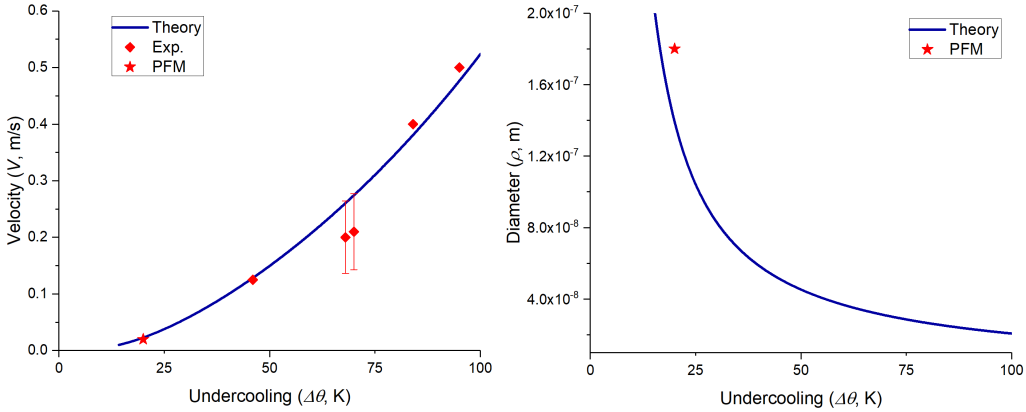

Figure 3. Dendrite tip velocity V and diameter ρ as functions of the melt undercooling $\Delta\theta$ for the alloy $Ni_{98}Zr_1Al_1$. The curves represent the theory under consideration. Experimental and PFM points are taken from Galenko et al. [58].

7. Conclusions

In summary, a new selection theory for a stable growth mode of dendritic crystals is developed with allowance for dissolved impurities and forced convection in an undercooled melt. The theory is developed for laminar viscous melt stream flowing around a dendrite, taking conductive heat and mass transfer on the crystal surface into account. Such crystal growth conditions correspond to the melt undercooling less than or of the order of 10^2 K. At a greater undercooling, the kinetic effects of atoms attachment to the dendrite solid-liquid interface should be taken into account. This, in particular, leads to the kinetic undercooling in the undercooling balance condition and essential corrections in the selection criterion (see, among others, Ref. [20], where these contributions have been considered for a two-component system). For even more undercooling greater than 2×10^2 K, the effects of local-nonequilibrium crystallization play a decisive role (the diffusion equations become of a hyperbolic type, the partition coefficients and liquidus slopes become dependent on the growth velocity V, and the undercooling balance and selection criterion essentially change (see, among others, refs. [20,35])). Keeping this in mind, we expect to extend the present analysis for large undercoolings ($\gtrsim 10^2$ K) in the nearest future.

As a special note let us underline that the theory under consideration describes the growth of dendritic tip, which preserves its shape and evolves with the constant velocity V. As this takes place, the whole dendritic interface can propagate in unsteady manner whose velocity satisfies the boundary integral equation [38].

Author Contributions: Conceptualization, D.V.A. and L.V.T.; methodology, D.V.A., P.K.G. and L.V.T.; software, L.V.T., S.I.O. and P.K.G.; validation, L.V.T., S.I.O. and P.K.G.; formal analysis, D.V.A. and P.K.G.; investigation, D.V.A.; resources, P.K.G.; writing—original draft preparation, D.V.A. and L.V.T.; writing—review and editing, D.V.A., L.V.T. and P.K.G.; visualization, L.V.T. and S.I.O.; supervision, P.K.G. and D.V.A.; project administration, P.K.G.; funding acquisition, D.V.A. and L.V.T. All authors have read and agreed to the published version of the manuscript.

Funding: The present research work consists of theoretical, computational and experimental parts, which were supported by different financial sources. D.V.A. and P.K.G. acknowledge the Russian Science Foundation (Project No. 20-61-46013) for the obtaining of selection criteria, computer simulations, and comparison with experimental data. L.V.T. is grateful to the Foundation for the Advancement of Theoretical Physics and Mathematics "BASIS" (project No. 21-1-3-11-1) for the development of a small piece of this study—the microscopic solvability condition (17).

Data Availability Statement: All data generated or analysed during this study are included in this published article.

Conflicts of Interest: The authors declare no conflict of interest.

Appendix A

Let us now generalize the selection criterion (26) for N-component dilute melt. Keeping in mind that contributions from additional impurities are additive within the framework of linear theory, we obtain

$$\sigma^* = \frac{2d_0D_\theta}{\rho^2 V} = \frac{\sigma_{0n}\chi_d^{7/n}B_n^{7/n}}{1+\beta\bar{v}_n^{s_n}}\left\{\frac{1}{\left[1+b_{1n}\chi_d^{2/n}B_n^{2/n}P_\theta\right]^2}+\sum_{j=1}^{N}\frac{2(1-k_j)m_j\sigma_{ji}D_\theta}{\left[1+b_{2n}\chi_d^{2/n}B_n^{2/n}P_{j\sigma}\right]^2 D_j\theta_Q}\right\}, \tag{A1}$$

where

$$\bar{v}_n = \left(\frac{b(\Re)ud_0}{4V\rho R}+\sum_{j=1}^{N}\frac{b(\Re)ud_0D_\theta}{2V\rho RD_j}\right)\chi_d^{-3/n}B_n^{-3/n},$$

$$R = 1+\sum_{j=1}^{N}\frac{2(1-k_j)m_j\sigma_{ji}D_\theta}{D_j\theta_Q},\quad P_{j\sigma}=\frac{\rho V}{2D_j}$$

with D_j being the diffusion coefficient of j-component of impurity.

An important point is that the selection criterion (A1) coincides with the previously developed criterion for a multicomponent system with four-fold crystalline symmetry without convection [57].

References

1. Meirmanov, A.M. *The Stefan Problem*; De Gruyter Expositions in Mathematics; De Gruyter: Berlin, Germany, 1992.
2. Pelcé, P. *Dynamics of Curved Fronts*; Academic Press: Boston, MA, USA, 1988.
3. Alexandrov, D.V.; Ivanov, A.A. The Stefan problem of solidification of ternary systems in the presence of moving phase transition regions. *J. Exp. Theor. Phys.* **2009**, *108*, 821–829. [CrossRef]
4. Buyevich, Y.A.; Alexandrov, D.V.; Mansurov, V.V. *Macrokinetics of Crystallization*; Begell House Inc.: New York, NY, USA, 2001.
5. Herlach, D.; Galenko, P.; Holland-Moritz, D. *Metastable Solids from Undercooled Melts*; Elsevier: Amsterdam, The Netherlands, 2007.
6. Asta, M.; Beckermann, C.; Karma, A.; Kurz, W.; Napolitano, R.; Plapp, M.; Purdy, G.; Rappaz, M.; Trivedi, R. Solidification microstructures and solid-state parallels: Recent developments, future directions. *J. Acta Mater.* **2009**, *57*, 941–971. [CrossRef]
7. Alexandrova, I.V.; Alexandrov, D.V.; Aseev, D.L.; Bulitcheva, S.V. Mushy layer formation during solidification of binary alloys from a cooled wall: The role of boundary conditions. *Acta Phys. Pol. A* **2009**, *115*, 791–794. [CrossRef]
8. Funke, O.; Phanikumar, G.; Galenko, P.K.; Chernova, L.; Reutzel, S.; Kolbe, M.; Herlach, D.M. Dendrite growth velocity in levitated undercooled nickel melts. *J. Cryst. Growth* **2006**, *297*, 211–222. [CrossRef]
9. Huppert, H.E. The fluid mechanics of solidification. *J. Fluid Mech.* **1990**, *212*, 209–240. [CrossRef]
10. Worster, M.G. Solidification of an alloy from a cooled boundary. *J. Fluid Mech.* **1986**, *167*, 481–501. [CrossRef]
11. Galenko, P.K.; Zhuravlev, V.A. *Physics of Dendrites*; World Scientific: Singapore, 1994.
12. Nizovtseva, I.G.; Alexandrov, D.V. The effect of density changes on crystallization with a mushy layer. *Phil. Trans. R. Soc. A* **2020**, *378*, 20190248. [CrossRef]

13. Skripov, V.P. *Metastable Liquids*; Wiley: New York, NY, USA, 1974.
14. Kelton, K.F.; Greer, A.L. *Nucleation in Condensed Matter: Applications in Materials and Biology*; Elsevier: Amsterdam, The Netherlands, 2010.
15. Makoveeva, E.V.; Alexandrov, D.V. Mathematical simulation of the crystal nucleation and growth at the intermediate stage of a phase transition. *Russ. Metall.* **2018**, *2018*, 707–715. [CrossRef]
16. Toropova, L.V.; Alexandrov, D.V. Dynamical law of the phase interface motion in the presence of crystals nucleation. *Sci. Rep.* **2022**, *12*, 10997. [CrossRef]
17. Toropova, L.V.; Aseev, D.L.; Osipov, S.I.; Ivanov, A.A. Mathematical modeling of bulk and directional crystallization with the moving phase transition layer. *Math. Methods Appl. Sci.* **2022**, *45*, 8011–8021. [CrossRef]
18. Ivantsov, G.P. Temperature field around spherical, cylinder and needle-like dendrite growing in supercooled melt. *Dokl. Akad. Nauk SSSR* **1947**, *58*, 567–569.
19. Ivantsov, G.P. On a growth of spherical and needle-like crystals of a binary alloy. *Dokl. Akad. Nauk SSSR* **1952**, *83*, 573–575.
20. Alexandrov, D.V.; Galenko, P.K. A review on the theory of stable dendritic growth. *Phil. Trans. R. Soc. A* **2021**, *379*, 20200325. [CrossRef]
21. Nash, G.E.; Glicksman, M.E. Capillary-limited steady-state dendritic growth I. Theoretical development. *Acta Metall.* **1974**, *22*, 1283–1290. [CrossRef]
22. Langer, J.S.; Muller-Krumbhaar, H. Theory of dendritic growth–I. Elements of a stability analysis. *Acta Metall.* **1978**, *26*, 1681–1687. [CrossRef]
23. Willnecker, R.; Herlach, D.; Feuerbacher, B. Evidence of nonequilibrium processes in rapid solidification of undercooled metals. *Phys. Rev. Lett.* **1989**, *62*, 2707–2710. [CrossRef]
24. Alexandrov, D.V.; Galenko, P.K. The shape of dendritic tips. *Phil. Trans. R. Soc. A* **2020**, *378*, 20190243. [CrossRef]
25. Alexandrov, D.V.; Toropova, L.V.; Titova, E.A.; Kao, A.; Demange, G.; Galenko, P.K.; Rettenmayr, M. The shape of dendritic tips: A test of theory with computations and experiments. *Phil. Trans. R. Soc. A* **2021**, *379*, 20200326. [CrossRef]
26. Toropova, L.V. Shape functions for dendrite tips of SCN and Si. *Eur. Phys. J. Spec. Top.* **2022**, *231*, 1129–1133. [CrossRef]
27. Toropova, L.V.; Alexandrov, D.V.; Rettenmayr, M.; Liu, D. Microstructure and morphology of Si crystals grown in pure Si and Al-Si melts. *J. Condens. Matter Phys.* **2022**, *34*, 094002. [CrossRef]
28. Kessler, D.A.; Koplik, J.; Levine, H. Pattern selection in fingered growth phenomena. *Adv. Phys.* **1988**, *37*, 255–339. [CrossRef]
29. Brener, E.A.; Mel'nikov, V.I. Pattern selection in two-dimensional dendritic growth. *Adv. Phys.* **1991**, *40*, 53–97. [CrossRef]
30. Alexandrov, D.V.; Galenko, P.K. Selected mode of dendritic growth with n-fold symmetry in the presence of a forced flow. *EPL* **2017**, *119*, 16001. [CrossRef]
31. Bouissou, P.; Pelcé, P. Effect of a forced flow on dendritic growth. *Phys. Rev. A* **1989**, *40*, 6637–6680. [CrossRef]
32. Ben Amar, M.; Pelcé, P. Impurity effect on dendritic growth. *Phys. Rev. A* **1989**, *39*, 4263–4269. [CrossRef]
33. Alexandrov, D.V.; Galenko, P.K. Selection criterion of stable dendritic growth at arbitrary Péclet numbers with convection. *Phys. Rev. E* **2013**, *87*, 062403. [CrossRef]
34. Alexandrov, D.V.; Galenko, P.K. Selection criterion of stable mode of dendritic growth with n-fold symmetry at arbitrary Péclet numbers with a forced convection. In *IUTAM Symposium on Recent Advances in Moving Boundary Problems in Mechanics*; Springer: Cham, Switzerland, 2019; pp. 203–215.
35. Alexandrov, D.V.; Galenko, P.K. Selected mode for rapidly growing needle-like dendrite controlled by heat and mass transport. *Acta Mater.* **2017**, *137*, 64–70. [CrossRef]
36. Alexandrov, D.V.; Dubovoi, G.; Malygin, A.P.; Nizovtseva, I.G.; Toropova, L.V. Solidification of ternary systems with a nonlinear phase diagram. *Russ. Metall.* **2017**, *2017*, 127–135. [CrossRef]
37. Alexandrov, D.V.; Alexandrova, I.V.; Ivanov, A.A.; Malygin, A.P.; Starodumov, I.O.; Toropova, L.V. On the theory of the nonstationary spherical crystal growth in supercooled melts and supersaturated solutions. *Russ. Metall.* **2019**, *2019*, 787–794. [CrossRef]
38. Alexandrov, D.V.; Galenko, P.K. Boundary integral approach for propagating interfaces in a binary non-isothermal mixture. *Phys. A Stat. Mech. Appl.* **2017**, *469*, 420–428. [CrossRef]
39. Bloomfield, L.J.; Huppert, H.E. Solidification and convection of a ternary solution cooled from the side. *J. Fluid Mech.* **2003**, *489*, 269–299. [CrossRef]
40. Anderson, D.M. A model for diffusion-controlled solidification of ternary alloys in mushy layers. *J. Fluid Mech.* **2003**, *483*, 165–197. [CrossRef]
41. Anderson, D.M.; Schulze, T.P. Linear and nonlinear convection in solidifying ternary alloys. *J. Fluid Mech.* **2005**, *545*, 213–243. [CrossRef]
42. Alexandrov, D.V.; Ivanov, A.A. Solidification of a ternary melt from a cooled boundary, or nonlinear dynamics of mushy layers. *J. Int. J. Heat Mass Trans.* **2009**, *21–22*, 4807–4811. [CrossRef]
43. Toropova, L.V.; Ivanov, A.A.; Osipov, S.I.; Yang, Y.; Makoveeva, E.V.; Alexandrov, D.V. Solidification of ternary melts with a two-phase layer. *J. Phys. Condens. Matter* **2022**, *34*, 383002. [CrossRef]
44. Lamb, H. *Hydrodynamics*; Dover Publications: New York, NY, USA, 1945.
45. Kochin, N.E.; Kibel, I.A.; Roze, N.V. *Theoretical Hydromechanics*; Interscience: New York, NY, USA, 1964.
46. Buyevich, Y.A.; Alexandrov, D.V.; Zakharov, S.V. *Hydrodynamics. Examples and Problems*; Begell House: New York, NY, USA, 2001.

47. Alexandrov, D.V.; Galenko, P.K. Dendritic growth in an inclined viscous flow. Part 1. Hydrodynamic solutions. *AIP Conf. Proc.* **2017**, *1906*, 200003.
48. Alexandrov, D.V.; Galenko, P.K. Dendritic growth in an inclined viscous flow. Part 2. Numerical examples. *AIP Conf. Proc.* **2017**, *1906*, 200004.
49. Pelcé, P.; Bensimon, D. Theory of dendrite dynamics. *Nucl. Phys. B* **1987**, *2*, 259–270. [CrossRef]
50. Titova, E.A.; Galenko, P.K.; Alexandrov, D.V. Method of evaluation for the non-stationary period of primary dendritic crystallization. *J. Phys. Chem. Solids* **2019**, *134*, 176–181. [CrossRef]
51. Langer, J.S.; Hong, D.C. Solvability conditions for dendritic growth in the boundary-layer model with capillary anisotropy. *Phys. Rev. A* **1986**, *34*, 1462–1471. [CrossRef]
52. Barbieri, A.; Langer, J.S. Predictions of dendritic growth rates in the linearized solvability theory. *Phys. Rev. A* **1989**, *39*, 5314–5325. [CrossRef]
53. Alexandrov, D.V.; Galenko, P.K. Thermo-solutal and kinetic regimes of an anisotropic dendrite growing under forced convective flow. *Phys. Chem. Chem. Phys.* **2015**, *17*, 19149–19161. [CrossRef]
54. Alexandrov, D.V.; Galenko, P.K. Dendritic growth with the six-fold symmetry: Theoretical predictions and experimental verification. *J. Phys. Chem. Solids* **2017**, *108*, 98–103. [CrossRef]
55. Toropova, L.V.; Alexandrov, D.V.; Rettenmayr, M.; Galenko, P.K. The role of intense convective flow on dendrites evolving with n-fold symmetry. *J. Cryst. Growth* **2020**, *535*, 125540. [CrossRef]
56. Alexandrov, D.V.; Galenko, P.K. Dendrite growth under forced convection: Analysis methods and experimental tests. *Phys.-Uspekhi* **2014**, *57*, 771–786. [CrossRef]
57. Alexandrov, D.V.; Pinigin, D.A. Selection of stable growth conditions for the parabolic dendrite tip in crystallization of multicomponent melts. *Tech. Phys.* **2013**, *58*, 309–315. [CrossRef]
58. Galenko, P.K.; Reutzel, S.; Herlach, D.M.; Fries, S.G.; Steinbach, I.; Apel, M. Dendritic solidification in undercooled Ni–Zr–Al melts: Experiments and modeling. *Acta Mater.* **2009**, *57*, 6166–6175. [CrossRef]
59. Zhao, Y.; Zhang, B.; Hou, H.; Chen, W.; Wang, M. Phase-field simulation for the evolution of solid/liquid interface frontin directional solidification process. *J. Mater. Sci. Technol.* **2019**, *35*, 1044–1052. [CrossRef]
60. Zhao, Y.; Liu, K.; Hou, H.; Chen, L.-Q. Role of interfacial energy anisotropy in dendrite orientation in Al-Zn alloys: A phase field study. *Mater. Des.* **2022**, *216*, 110555. [CrossRef]
61. Eiken, J.; Böttger, B.; Steinbach, I. Multiphase-field approach for multicomponent alloys with extrapolation scheme for numerical application. *Phys. Rev. E* **2006**, *73*, 066122. [CrossRef]